J Inorg Organomet Polym (2017) 27:1243–1251
DOI 10.1007/s10904-017-0571-3

An Extremely Stable 2D Zinc(II) Coordination Polymer Exhibiting High Sensing Ability and Photocatalytic Degradation Activities of Dyes

Yu Wu[1] · Jing Feng[2] · Bin Xie[1] · Like Zou[1] · Yulong Li[1] · Zhiquan Li[3]

Received: 15 March 2017 / Accepted: 2 May 2017 / Published online: 9 May 2017

Abstract A new 2D Zn(II) metal-organic framework of $\{[Zn(L)(4,4'\text{-bipy})\cdot CH_3CN]_n$ (**1**) has been developed using 5-aminoisophthalic acid (H_2L) and 4,4′-bipyridine ligands. The single crystal X-ray diffraction study indicates that **1** is composed of infinite 2D layer. The chemically stable **1** behaves as a highly selective and sensitive fluorescence chemosensor for detection of Hg^{2+} and 4-nitrotoluene (4-NT) analyte. Furthermore, the photocatalytic properties of **1** for degradation of the methyl violet (MV) and Rhodamine B (RhB) have been explored.

Keywords Fluorescence · Chemosensor · Photocatalysis · Structure

1 Introduction

Recently, there is an increasing trend in using luminescence MOFs to probe guest species and thus develop multifunctional MOFs that combine luminescence and other promising applications [1–15]. Research studies have been focused on the luminescent sensing materials for Cu^{2+}, Fe^{3+} and small organic molecules known as environmental pollutants [16–23]. However, only a few examples of MOFs were associated with the luminescent probe for Hg^{2+}ions, which shows serious environmental and health problems due to its toxic effects [17, 24–27]. In these studies, the competing selectivity to $Hg^{2+}$was discussed, not work on the recyclable and removal performance of Hg^{2+} sensors were carried out.

On the other hand, some fascinating MOFs [such as UIO-66 and MIL-100(Fe)] have already been demonstrated and showed excellent semiconductor properties for photocatalysis [28–33]. Degradation of organic molecules with MOFs has advantages because the associated reactions could take place at similar rates both at the internal and external surfaces of photocatalysts. Furthermore, MOF-based photocatalysts with high stability are always expected to maximize the efficiency of their actions, which will be helpful to facilitate convenient recycling of the used photocatalysts [34–42].

To achieve useful MOF sensors, an effective method is to use the ligand-based strategy containing π-conjugated rigid organic ligands [43]. In our previous effort, we have synthesized some multifunctional MOFs with excellent properties [44–46]. Herein, the rigid 5-aminoisophthalic acid (H_2L), 4,4′-bipyridine (4,4′-bipy), and transition-metal center (Zn^{II}) were selected to construct new structures with potential applications in luminescence sensing and photocatalysis based on the following considerations: (1) the

Electronic supplementary material The online version of this article (doi:10.1007/s10904-017-0571-3) contains supplementary material, which is available to authorized users.

✉ Yu Wu
wuyuhlj@163.com

✉ Zhiquan Li
lizq1975@163.com

[1] School of Chemistry and Environmental Engineering, Sichuan University of Science & Engineering, Zigong 643000, People's Republic of China

[2] Department of Mechanical and Electrical Engineering, Guangdong University of Science & Technology, Dongguan 523083, People's Republic of China

[3] PLA Institute of Orthopedics & Traumatology, Xijing Hospital, The Fourth Military Medical University, Xi'an 710032, People's Republic of China

Table 1 Crystal data and structure refinement information for compound **1**

Parameter	**1**
Formula	$C_{15}H_{12}ZnN_3O_4$
Formula weight	363.65
Crystal system	Monoclinic
Space group	P21/c
Crystal color	Brown
a, [Å]	12.1860(6)
b, [Å]	7.6743(4)
c, [Å]	16.1059(7)
α, [°]	90.00
β, [°]	108.901(1)
γ, [°]	90.00
V, Å^3	1424.99(12)
Z	4
ρ_{calcd}, g/cm^3	1.695
μ, mm^{-1}	1.748
F(000)	740
θRange, deg	2.97–25.01
Reflection collected	2220/2506
Goodness-of-fit on F^2	1.087
R_1, $wR_2(I>2\sigma(I))$[a]	0.0469, 0.1277
R_1, wR_2 (all data)[b]	0.0518, 0.1328

[a] $R=\sum(F_o-F_c)/\sum(F_o)$

[b] $wR_2=\{\sum[w(F_o^2-F_c^2)^2]/\sum(F_o^2)^2\}^{1/2}$

binding between H_2L and metal centers will alter the electronic structures and surface functionalities of the MOFs, which may induce their specific recognition for guest substrates through host–guest interactions; (2) rigid ligand H_2L and 4,4′-bipy with aromatic π rings may effectively favor intraligand interactions and promote luminescent characterities. We present a new MOF in this work, namely, {[Zn(L)(4,4′-bipy)·CH_3CN]$_n$ (**1**), which exhibits a 2D layer network. **1** behaves as a highly selective and sensitive sensor for detection of Hg^{2+} ions and explosives (4-nitrotoluene). Furthermore, the photocatalytic properties of **1** for degradation of the methyl violet (MV) and Rhodamine B (Rh B) have been explored.

2 Materials and Methods

All the other reagents used for the syntheses were commercially available and employed without further purification. Powder X-ray diffraction (PXRD) was collected on a Bruker ADVANCE X-ray diffractometer with Cu-Kα radiation (λ = 1.5418 Å) at 50 kV, 20 mA with a scanning rate of 6°/min and a step size of 0.02°. Fourier transform infrared (FT-IR) spectra as KBr pellets were measured using a Nicolet Impact 750 FTIR in the range of 400–4000 cm^{-1}. Thermogravimetric analysis was performed under N_2 atmosphere from room temperature to 900 °C at a heating rate of 10 °C min^{-1}. The photocatalytic activity studies were carried out in a Shimadzu UV–Vis 2501PC recording spectrophotometer.

2.1 X-ray Crystallography

The single crystal X-ray diffraction data were collected on a Bruker SMART APEX diffractometer that was equipped with graphite monochromated MoKα radiation (λ = 0.71073 Å) by using an ω-scan technique. The intensities were corrected for absorption effects by using SADABS [47]. The structure was solved using SHELXL-97 [48]. All the hydrogen atoms were generated geometrically and refined isotropically using a riding model. All non-hydrogen atoms were refined with anisotropic displacement parameters. Crystallographic details and selected bond dimensions for **1** are listed in Tables 1 and 2, respectively. CCDC number: 1536142.

2.2 Synthesis of 1

A mixture of $Zn(NO_3)_2{\cdot}6H_2O$ (0.029 g, 0.1 mmol), 5-aminoisophthalic acid (0.019 g, 0.1 mmol), 4,4′-bipyridine(0.016 g, 0.1 mmol), CH_3CN (3 mL) and deionised water (3 mL) was stirred for 30 min in air. The resulting solution was placed in a Teflon-lined stainless steel vessel (25 mL) and heated to 160 °C for 72 h, brown block crystals of **1** were obtained. (Yield 58% based on Zn). Anal. Calcd(%) for $C_{15}H_{12}ZnN_3O_4$, C, 49.54; H, 3.33; N, 11.55. Found C, 49.34; H, 3.15; N, 11.49. IR: 3100 (m); 1833 (m); 1624 (vs); 1561 (vs); 1478 (v); 1430 (m); 1357 (vs); 1233 (m); 1096 (m); 966 (v); 782 (v); 731 (m); 647 (vs).

2.3 Photocatalytic Method

The photocatalytic reactions were performed as follows: 50 mg of **1** were dispersed in 50 mL aqueous solution of MV (10 mg/L) under stirring in the dark for 30 min to ensure the establishment of an adsorption–desorption equilibrium. Then the mixed solution was exposed to UV

Table 2 Selected bond distances (Å) and angles (°) of structure **1**

Zn(1)–O(3)	1.940 (3)	Zn(1)–O(2)#1	1.986 (2)
Zn(1)–N(2)	2.045 (3)	Zn(1)–N(1)#2	2.098 (3)
O(2)#1–Zn(1)–O(3)	102.85 (11)	O(3)–Zn(1)–N(2)	104.95 (13)
O(2)#1–Zn(2)–N(2)	130.70 (13)	O(3)–Zn(1)–N(1)#2	109.95 (12)
O(2)#1–Zn(1)–N(1)#2	103.43 (12)	N(2)–Zn(1)–N(1)#2	104.16 (12)

Symmetry codes: #1: x, 0.5 − y, 0.5 + z; #2: x, 1.5 − y, 0.5 + z

irradiation from an Hg lamp (250 W) and kept under continuous stirring during irradiation for 100 min. Samples of 5 mL were taken out every 10 min and collected by centrifugation for analysis by UV–Vis spectrometer. By contrast, the simple control experiment was also performed under the same condition without adding any catalysts.

2.4 Sensing Method

The photoluminescence sensing were performed as follows: the photoluminescence properties of **1** were investigated in *N*,*N*-dimethylformamide (DMF) dispersions at room temperature using a RF-5301PC spectrofluorophotometer. The **1**@DMF emulsions were prepared by adding 3 mg of **1** powder into 3.00 mL of DMF and then ultrasonic agitation the mixture for 30 min before testing. The fluorescence spectra were recorded 5 min after adding the appropriate amount of M^{2+} stock solution. This exposure time ensured that analyte interacted completely with **1**. Each measurement was repeated three times, and the average value was used.

3 Results and Discussion

3.1 Crystal Structures

$$\left\{\left[Zn(L)\left(4,4'-bipy\right)\cdot CH_3CN\right]_n\right\}(\mathbf{1})$$

Single-crystal X-ray diffraction analysis reveals that **1** crystallizes in the monoclinic space group $P2_1/c$ (Table 1). Its asymmetric unit contains one Zn(II), one L^{2-}, one 4,4′-bipy, and a crystallization CH_3CN molecule. Zn1 shows a trigonal bipyramid geometry, being defined by three O atoms of two carboxylate groups from two L^{2-}, one N atom from amino group from L^{2-} ligand and one N atom from 4,4′-bipy (Fig. 1a). The crystallographically independent L^{2-} exhibits a tridentate coordination mode linking three Zn(II) centers with one monodentate and one bidentate carboxylate groups and one amino group, forming a 1D chain (Fig. 1b). The carboxylate groups and the central benzene ring are not in a plane with the average dihedral angle of 87.9°. Interestingly, the 1D chain contains a 22-membered.

metallo-macrocycles made up of three L and three zinc ions. Furthermore, the 1D chain are infinitely connected

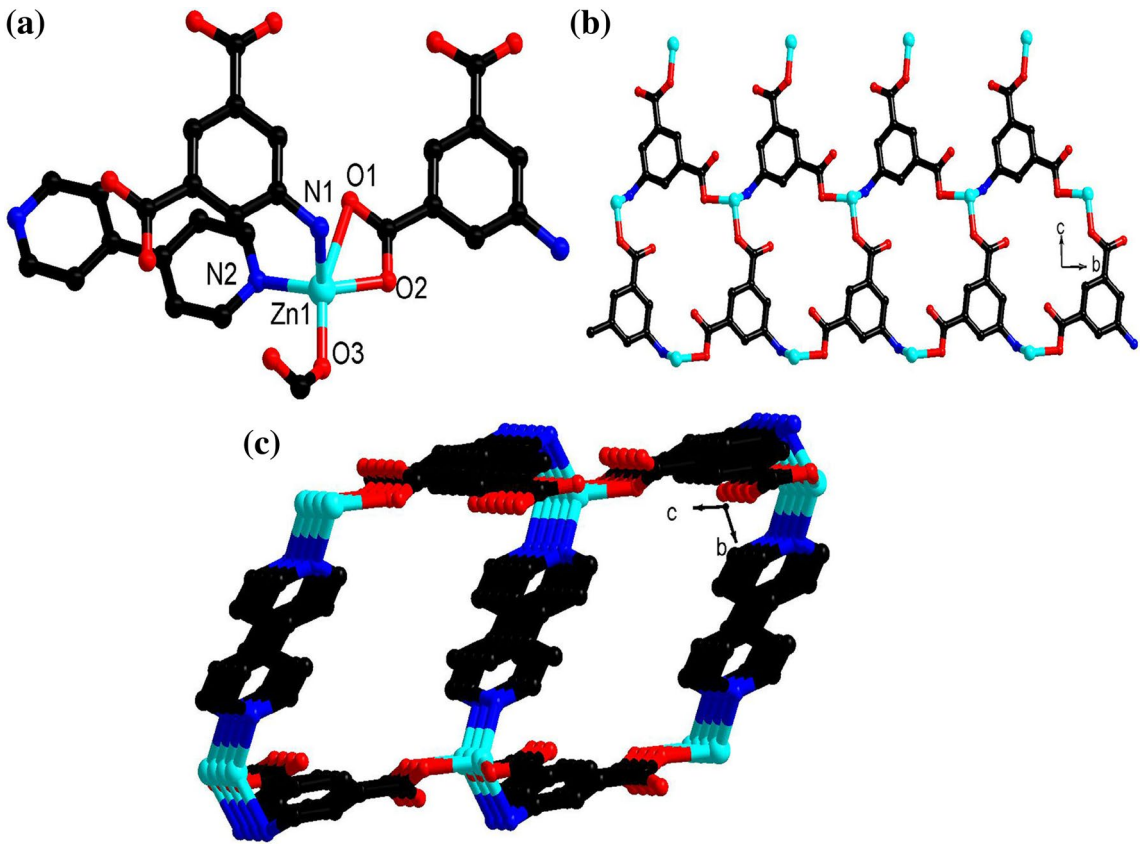

Fig. 1 **a** View of the coordination environment of Zn^{2+} center; **b** 1D chain constructed by metal centers and L ligands; **c** 2D layer along the *bc*-plane

by bridging 4,4′-bpy ligand to generate a 2D layer structure, as shown in Fig. 2c. A similar structure has been also observed in CPO-8-DEF series [49].

As we expect, the single crystals of **1** remain unchanged in air for a very long time as expected. To further investigate the stability of **1**, it was soaked in aqueous solutions with different pH values. Powder X-ray diffraction (XRD) patterns, IR and TGA data have unambiguously demonstrated that the crystallinity and framework integrity of **1** can be well retained at the range of pH 2–12 (Fig. 2a; Fig. S7, S8), setting **1** among the most stable MOFs that is tolerable wide pH ranges as far as possible [50]. It is believed that the exceptional stability of **1** is attributed to the strong Zn–N bonds from amino group [51–57]. Undoubtedly, the great stability of **1** provides the structure integrity during its application performances.

3.2 Luminescence Sensing

Taking into account the excellent luminescent properties of MOFs composed of d^{10} metal centers and electron-rich π-conjugated ligands [58, 59], the fluorescence behaviors of **1**, H_2L and 4,4′-bipy ligands were investigated at room temperature. The free H_2L ligand exhibits emission at 420 nm ($\lambda_{ex}=300$ nm). The 4,4′-bipy exhibits emission at 350 nm ($\lambda_{ex}=290$ nm). It has been reported that

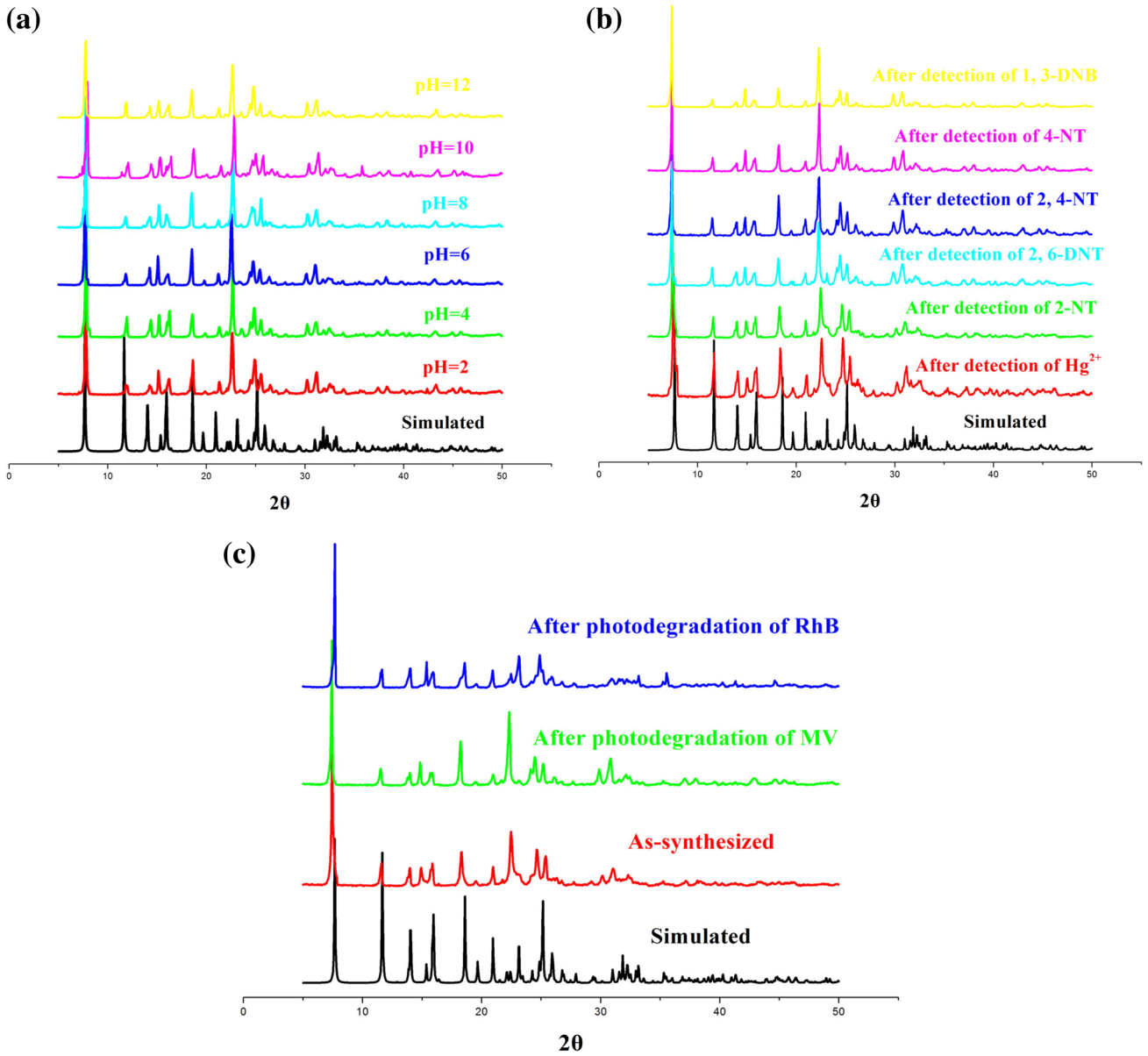

Fig. 2 **a–c** Powder XRD profiles of **1** at different pH, after fluorescence sensing and photocatalysis, respectively

the fluorescence feature of 4,4′-bipy can be omitted due to its backbone [58, 59]. Thus, compared to the luminescent spectra of the free H_2L ligand, **1** has a similar emission at 421 nm ($\lambda_{ex}=290$ nm) (Fig. S1), which may mostly attributed to the emission of the organic linker [13, 24, 60–65]. Thus, it is expected that compound **1** can show excellent performance on sensing nitroaromatics (NACs) based on their luminescence properties and highly chemical stability. The luminescence intensities of **1** closely depend on the solvents, it was found that complete luminescence quenching observed in NB solvent, which indicates **1** as luminescence sensor to detect NACs (Fig. S2). With these in mind, some more NACs including, 2-nitrotoluene (2-NT), 4-nitrotoluene (4-NT), 1,3-dinitrobezene (1,3-DNB), 2,4-dinitrotoulene (2,4-DNT) and 2,6-dinitrotoulene (2,6-DNT), and nitrobenzene (NB) have been selected for evaluating sensibility of **1**. In term of the luminescence quenching, it is found that **1** is capable of sensing all above NACs with the quenching efficacy increasing with concentration of NACs (Fig. 3; Fig. S3). The order of quenching efficiency is 4-NT > NB > 2,4-DNT > 1,3-DNB > 2-NT > 2,6-DNT. This efficiency is comparable to that of other MOFs in sensing 4-NT. The quenching constant (K_{SV}) of **1** for NT in the low concentration range is 3.59×10^4 M^{-1}, (Fig. S4), which is comparable to some of the recent examples of MOF-based sensors, such as [Eu3(bpydb)3(HCOO)(μ3-OH)2(H2O)] (2.1×104 M−1), [Cd(NDC)0.5(PCA)] (3.5×104 M−1), [Tb(1,3,5-BTC)] (3.42×104 M−1) and UiO-67-dcppy (2.9×104 M−1) [13, 62–64]. Considering the sizes of nitroaromatic compounds and the absence of large pores in this MOF, we can neglect the possibility of the accommodation of analytes in the pores. The luminescence attenuation could be attributed to the polarizability of analytes in an DMF solution and the π–π interaction between the analytes and the host framework [24, 65]. It reveals that **1** exhibit the high sensitivity to the nitro 4-NT with limit of detection (LOD) at ppm level with 3.2 ppm based on a 3δ/slope [66]. To the best of our knowledge, the sensitivity of **1** for these 4-NT aromatics is higher than that most of reported MOFs [67]. Eventually, it is noteworthy that the post experiment framework integrity of **1** was well preserved as ascertained by its almost unchanged PXRD pattern compared to that of the original samples (Fig. 2b).

The luminescence spectrum and PXRD patterns for **1**, recycled after three consecutive runs, are consistent with those acquired for pristine compound (Fig. S5). The results indicate that the frameworks of **1** are still stable and can be recycled by a fast and simple method.

In order to explore the luminescent responses of **1** to metal ions, **1** was dispersed in DMF solutions containing different $M(NO_3)_x$ salts. The luminescent intensity of **1** is almost quenched the luminescence of **1** in the presence of Hg^{2+}, indicating highly selective sensing of Hg^{2+} by **1** through this quenching effect [68–71] (Fig. 4a). The PXRD patterns of **1** indicated their original frameworks are intact upon dispersion in the metal ion solutions (Fig. 2b). To quantitatively investigate the response behavior of **1** towards Hg^{2+} ions (Fig. 4b), the emission

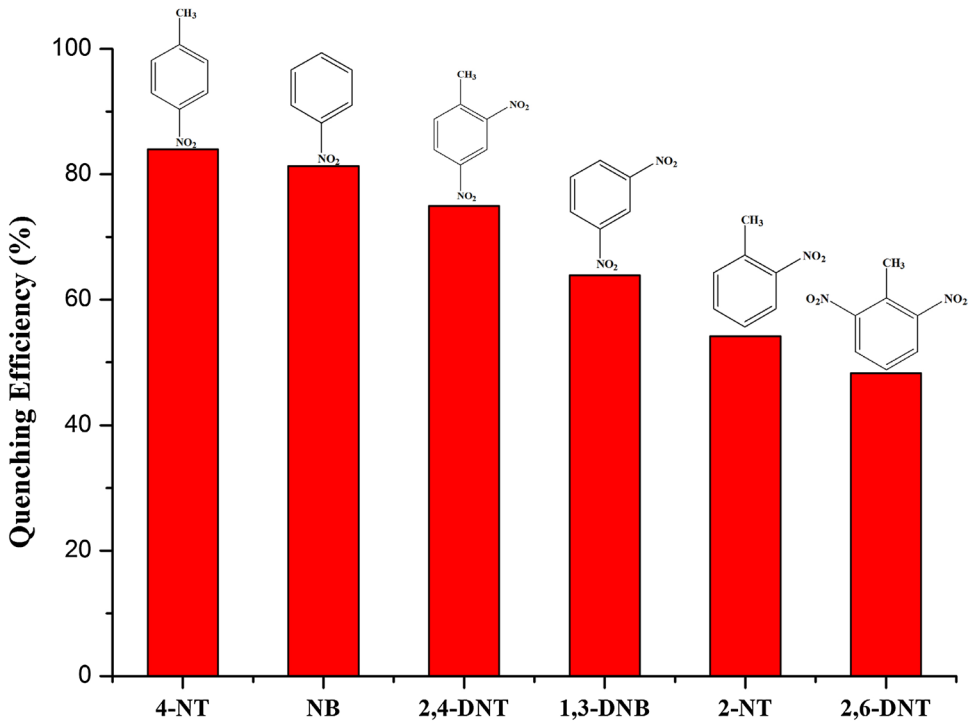

Fig. 3 The order of quenching efficiency of **1** in presence of different nitroaromatics with 4-NT, NB, 2,4-DNT,1,3-DNB, 2-NT, 2,6-DNT

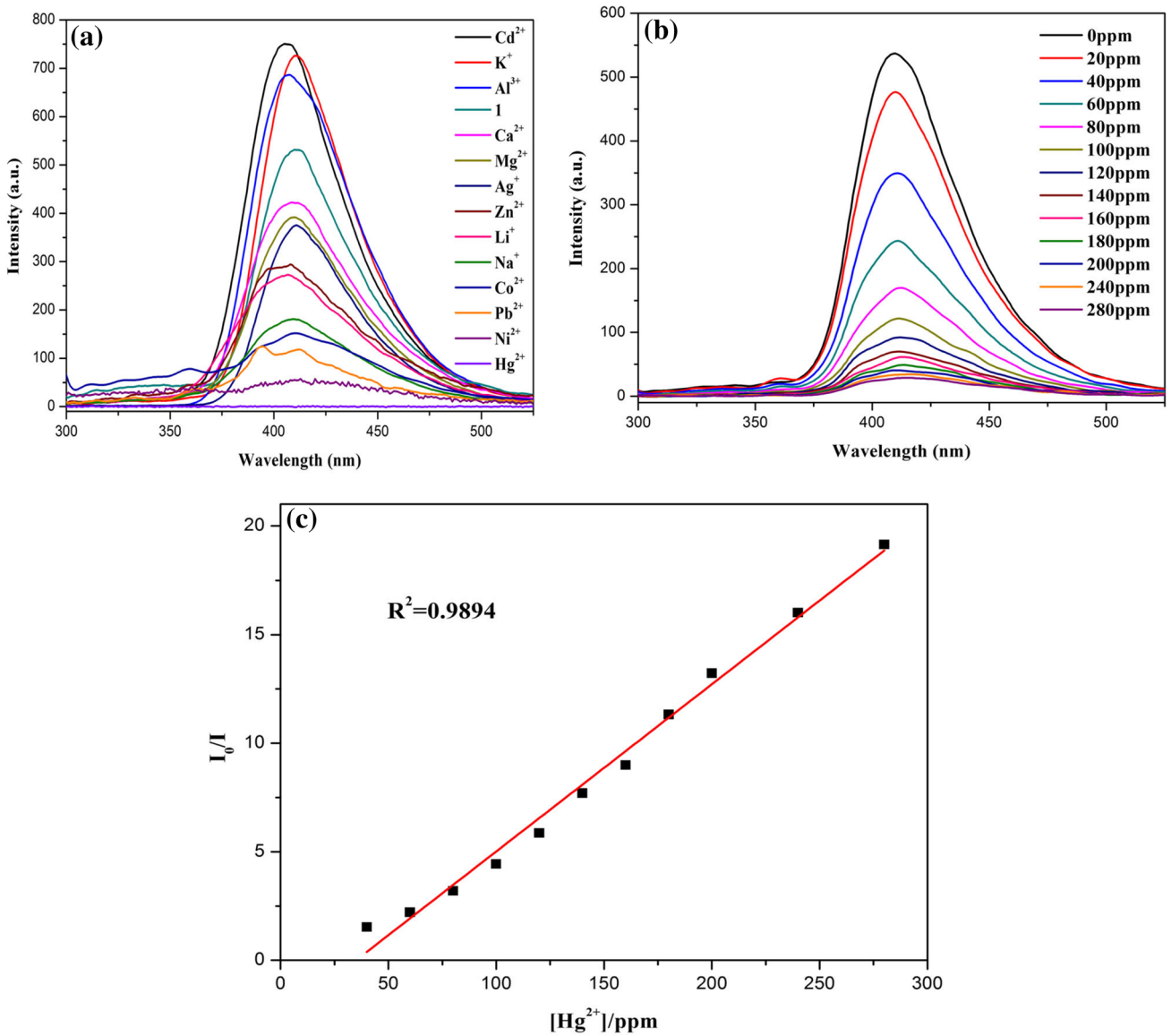

Fig. 4 **a** Fluorescence response of **1** to various anions in DMF (λ_{ex} = 290 nm); **b** fluorescence response of **1** in different concentrations of $Hg(NO_3)_2$ DMF solution; **c** views of Stern–Volmer plots

spectra of **1** in the presence of different concentrations of Hg^{2+} ions in DMF were measured at room temperature. The luminescent intensity of **1** is almost completely quenched at a $Hg(NO_3)_2$ concentration of 280 ppm. Furthermore, a linear correlation for $(I_0)/I$ and the concentration of Hg^{2+} ions was obtained, the detection limit of 1.11 ppm was calculated based on a 3δ/slope [66] (Fig. 4c; Table S1), which is relatively higher compared to reported examples [72, 73]. It was only found that the higher quenching efficiency for Hg^{2+} was the heavily studied PCN-224 [74–76]. Recently, Li et al., have reported a series of 3D Luminescent MOFs of LMOF-261, -262 and -263, which are extremely responsive to toxic heavy metals at a parts per billion level (3.3 ppb Hg^{2+}) [76]. Moreover, in all the analytes we used in this work, Hg^{2+} and explosives all have a strong absorbing range from 250 to 350 nm (Fig. S6), the strong absorption band of ligand is located at 285 nm, which is largely overlapped by the absorbing band of Hg^{2+} and explosives. Upon excitation, there is competition of the absorption of the light source energy between Hg^{2+} and explosives and H_2L from 250 to 350 nm. Combined with the absorption and luminescent spectra, it was suggested that the energy absorbed by the H_2L is transferred to the Hg^{2+} and explosives analytes, resulting in a decrease in the luminescence intensity. The quenching mechanism is in agreement with that proposed previously by Chen et al. [25].

3.3 Photocatalytic Activities

These methyl violet (MV) and Rhodamine B (RhB) were selected as model organic contaminant to study the photocatalytic activities of **1**. The absorption peaks of MV and RhB decrease obviously with the increasing of reaction time in the presence of **1** (Fig. 5a, b). The calculation results show that the degradation rates of MV and RhB are 60.6 and 29.4%, respectively (Fig. 5c). In addition, the control experiments on the degradation of organic pollutants were examined in the same reaction condition just without catalyst. The degradation rates of MV and RhB are just 18.8 and 14.3% within 100 min under UV irradiation without catalyst, respectively. So, the final structures of dyes may influence their degradation activities. In order to evaluate reproducible abilities of the as-synthesized photocatalysts, the repeated photocatalytic degradation of a constant MV concentration were discussed (Fig. 5d). The degradation rates of **1** showed no significant reduction when the photocatalysts were used three times in the same procedures, which suggests that the photocatalytic activities have well reproducibility. After photocatalysis, the PXRD patterns of **1** are similar with the simulated one, implying that **1** maintains its structural interlinkage after the photocatalysis reaction (Fig. 2c). Cheng and co-workers have designed and synthesized a series of Zn-MOFs with dicarboxylate ligands, which were used to degrade the methylene blue (MB) in polluted water. The final results show the catalytic performance of them may be ascribed to adsorption properties for MB and electronic charges on their solid surface. However, compared to above photocatalytic activity and presented in this work, the low photocatalytic activity of above compounds may be their flexible structural backbones, which may cause the relatively lower capture capability for MB [77]. Herein, these fact indicates that the title compound demonstrates excellent catalytic

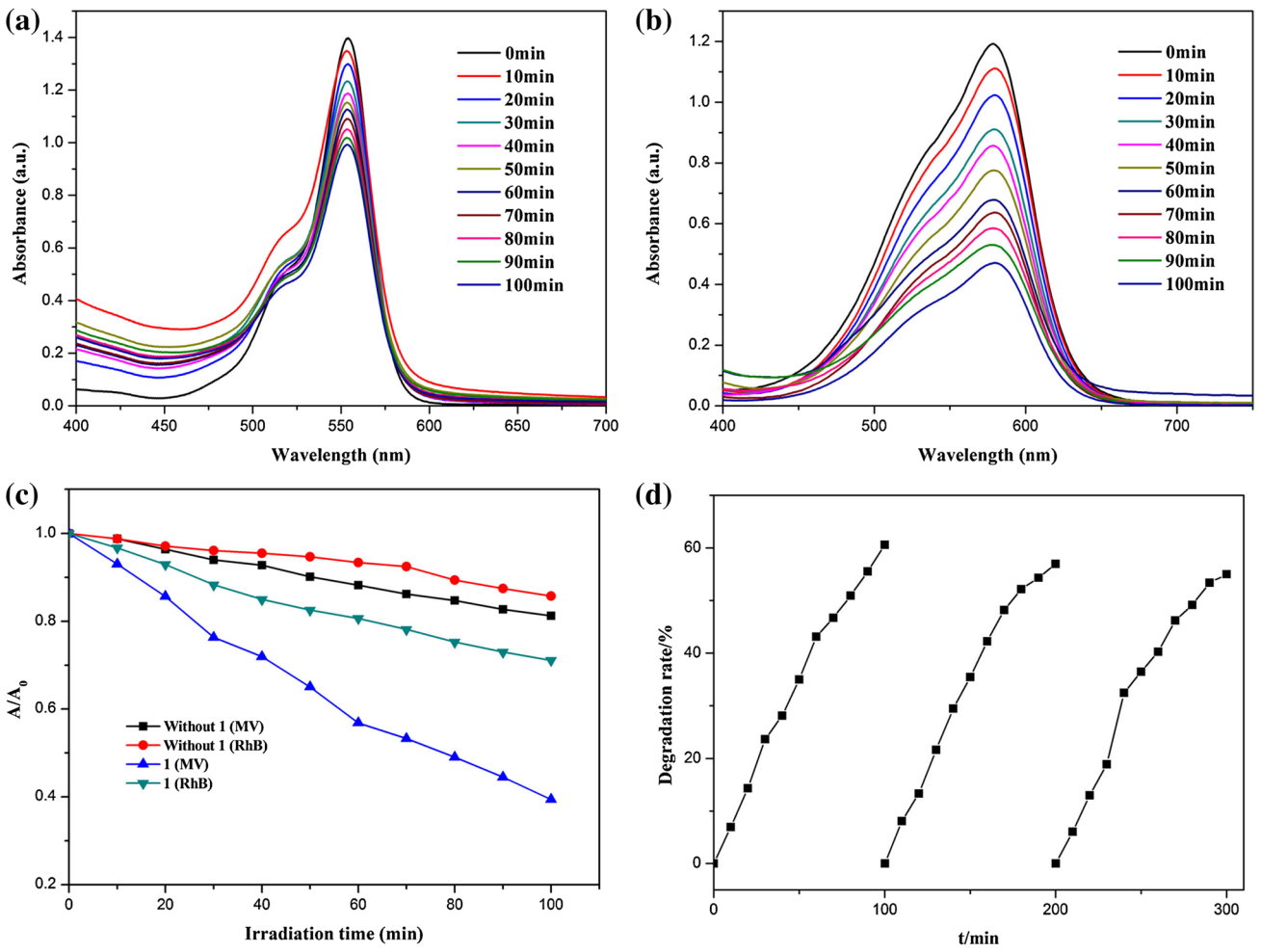

Fig. 5 **a, b** UV–Vis absorption spectra of the MV and RhB solution during the decomposition reaction under 500 W Hg lamp irradiation in the presence of **1**, respectively; **c** photodegradation of RhB and MV solution with the change in A/A_0 of **1**, and the control experiments without any catalyst; **d** recycling tests of **1** towards photodegradation of MV

activity and good stability for the photodegradation of dyes in water [78–83].

4 Conclusion

In summary, we have designed and synthesized chemically stable polymer **1**, which are well suitable for the simultaneous optical detection of metal ions and explosives through fluorescence quenching. Our title probe provided highly sensitive analyses of Hg^{2+} ion with an LOD of 1.11 ppm, and excellent selectivity with minor interference from other metal ions. Polymer **1** displays good photocatalytic activity for the degradation of MV under Hg-lamp, with a degradation rate of 60.6% within 100 min. The higher stability and recyclability of **1** make it outstanding candidates in the field of degradation of dyes as well as fluorescent probes.

Acknowledgements The authors acknowledge financial assistance from National Natural Science Foundation of China (21501124), the program of Science and Technology Department of Sichuan province (Nos. 2016JY0048, 2016GZ0172, 2017JY0194), the Opening Project of Key Laboratory of Green Catalysis of Sichuan Institutes of High Education (No. LZJ14201), the start-up foundation of Sichuan University of Science & Engineering (Nos. 2015RC23, 2015RC29, 2017RCL02), the Institute of Functionalized Materials (Nos. 2014PY01, 2015PY03), the Project of Zigong Science & Technology and Intellectual Property Bureau (Nos. 2014HX02, 2015HX16, 2015HX18).

References

1. L.L. Wen, X.Y. Xu, K.L. Lv, Y.M. Huang, X.F. Zheng, L. Zhou, R.Q. Sun, D.F. Li, ACS Appl. Mater. Interfaces **7**, 4449 (2015)
2. Y.L. Wu, G.P. Yang, Y.Q. Zhao, W.P. Wu, B. Liu, Y.Y. Wang, Dalton Trans. **44**, 3271 (2015)
3. J.Q. Liu, G.L. Liu, C.Y. Gu, W.C. Liu, J.W. Xu, B.H. Li, W.J. Wang, J. Mater. Chem. A **4**, 11630 (2016)
4. J.Q. Liu, J. Wu, F.M. Li, W.C. Liu, B.H. Li, J. Wang, Q.L. Li, R. Yadav, A. Kumar, RSC Adv. **6**, 31161 (2016)
5. B.H. Li, J. Wu, J.Q. Liu, C.Y. Gu, J.W. Xu, M.M. Luo, R. Yadav, A. Kumar, S.R. Batten, ChemPlusChem **81**, 885 (2016)
6. J.Q. Liu, G.P. Li, W.C. Liu, Q.L. Li, B.H. Li, R.W. Gable, L. Hou, S.R. Batten, ChemPlusChem **81**, 1299 (2016)
7. F.P. Zhai, M.L. Deng, Y. Ling, Z.X. Chen, Y.M. Zhou, Inorg. Chim. Acta **402**, 104 (2013)
8. X.Y. Dong, R. Wang, J.Z. Wang, S.Q. Zang, T.C.W. Mak, J. Mater. Chem. A **3**, 641 (2015)
9. B.L. Chen, L.B. Wang, Y.Q. Xiao, F.R. Fronczek, M. Xue, Y.J. Cui, G.D. Qian, Angew. Chem. Int. Ed. **48**, 500 (2009)
10. J. Lan, K.H. Li, H.H. Wu, D.H. Olson, T.J. Emge, W. Ki, M.C. Hong, J. Li, Angew. Chem. Int. Ed. **48**, 2334 (2009)
11. Z.G. Xie, L.Q. Ma, K.E. deKrafft, A. Jin, W.B. Lin, J. Am. Chem. Soc. **132**, 922 (2010)
12. Z. Hao, X. Song, M. Zhu, X. Meng, S. Zhao, S. Su, W. Yang, S. Song, H. Zhang, J. Mater. Chem. A **1**, 11043 (2013)
13. S.S. Nagarkar, B. Joarder, A.K. Chaudhari, S. Mukherjee, S.K. Ghosh, Angew. Chem. Int. Ed. **52**, 2881 (2013)
14. L.Y. Pang, G.P. Yang, J.C. Jin, M. Kang, A.Y. Fu, Y.Y. Wang, Q.Z. Shi, Cryst. Growth Des. **14**, 2954 (2014)
15. X.L. Hu, F.H. Liu, C. Qin, K.Z. Shao, M.Z., Su, Dalton Trans. **44**, 7822 (2015)
16. W.Y. Dan, X.F. Liu, M.L. Deng, Y. Ling, Z.X. Chen, M.Y. Zhou, Dalton Trans. **44**, 3794 (2015)
17. Z. Hu, B.J. Deibert, J. Li, Chem. Soc. Rev. **43**, 5815 (2014)
18. D. Banerjee, Z. Hu, J. Li, Dalton Trans. **43**, 10668 (2014)
19. Y. Salinas, R. Martinez-Manez, M.D. Marcos, F. Sancenon, A.M. Castero, M. Parra, S. Gil, Chem. Soc. Rev. **41**, 1261 (2012)
20. S.W. Thomas III, G.D. Joly, T.M. Swager, Chem. Soc. Rev. **36**, 1339 (2007)
21. D.T. McQuade, A.E. Pullen, T.M. Swager, Chem. Rev. **100**, 2537 (2000)
22. S.J. Toal, W.C. Trogler, J. Mater. Chem. **16**, 2871 (2006)
23. M.E. Germain, M.J. Knapp, Chem. Soc. Rev. **38**, 2543 (2009)
24. C.Q. Zhang, L.B. Sun, Y. Yan, J.Y. Li, X.W. Song, Y.L. Liu, Z.Q. Liang, Dalton Trans. **44**, 230 (2015)
25. B. Chen, L. Wang, Y. Xiao, F.R. Fronczek, M. Xue, Y. Cui, G. Qian, Angew. Chem. Int. Ed. **48**, 500 (2009)
26. Y. Cui, Y. Yue, G. Qian, B. Chen, Chem. Rev. **112**, 1126 (2012)
27. M.D. Allendorf, C.A. Bauer, R.K. Bhakta, R.J. Houk, Chem. Soc. Rev. **38**, 1330 (2009)
28. R. Kaur, K. Vellingiri, K.H. Kim, A.K. Paul, A. Deep, Chemosphere **154**, 620 (2016)
29. F.Q. Wang, C.M. Wang, Z.C. Yu, K.H. Xu, X.Y. Li, Y.Y. Fu, Polyhedron **105**, 49 (2016)
30. S.B. Wang, X.C. Wang, Small **11**, 3097 (2015)
31. Y.W. Gao, S.M. Li, Y.X. Li, L.Y. Yao, H. Zhang, Appl. Catal. B **202**, 165 (2017)
32. C.G. Silva, A. Corma, H. García, J. Mater. Chem. **20**, 3141 (2010)
33. M.C. So, G.P. Wiederrecht, J.E. Mondloch, J.T. Hupp, O.K. Farha, Chem. Commun. **51**, 3501 (2015)
34. F.X.L.I. Xamena, A. Corma, H. Garcia, J. Phys. Chem. C **111**, 80 (2006)
35. C. Wang, Z.G. Xie, K.E. Dekrafft, W. Lin, J. Am. Chem. Soc. **133**, 13445 (2011)
36. C.Y. Lee, O.K. Farha, B.J. Hong, A.A. Sarjeant, S.T. Nguyen, J.T. Hupp, J. Am. Chem. Soc. **133**, 15858 (2011)
37. C.G. Silva, I. Luz, F.X.L.I. Xamena, A. Corma, H. Garcia, Chem. Eur. J. **16**, 11133 (2010)
38. J.L. Wang, C. Wang, W.B. Lin, ACS Catal. **2**, 2630 (2012)
39. Z.A. Zong, X.M. Meng, X. Li, L.S. Cui, Y.H. Fan, J. Inorg. Organomet. Polym. Mater. **26**, 519 (2016)
40. C.C. Wang, J.R. Li, X.L. Lv, Y.Q. Zhang, G.S. Guo, Energy Environ. Sci. **7**, 2831 (2014)
41. J. Wang, W.J. Cui, An, K.V. Hecke, G.H. Cui, Dalton Trans. **45**, 17474 (2016)
42. S.Y. Hao, S.X. Hou, K.V. Hecke, G.H. Cui, Dalton Trans. **46**, 1951 (2017)
43. J.A. Hua, Y. Zhao, Y.S. Kang, Y. Lu, Y.W. Sun, Dalton Trans. **44**, 11524 (2015)
44. Y. Wu, Y.L. Li, L.K. Zou, J.S. Feng, J.Q. Liu, M.M. Luo, J.W. Xu, R. Yadav, A. Kumar, Z. Anorg. Allg. Chem. **643**, 214 (2017)
45. Y. Wu, J. Wu, Z.D. Luo, J. Wang, Y.L. Li, Y.Y. Han, Q.J. Liu, RSC Adv. **7**, 10415 (2017)
46. Y. Wu, J. He, S.Q. Wang, L.K. Zou, X.R. Wu, Inorg. Chim. Acta **458**, 218 (2017)
47. G.M. Sheldrick, *SADABS, Program for Siemens Area Detector Absorption Corrections* (University of Göttingen, Göttingen, 1997)
48. G.M. Sheldrick, *SADABS* (University of Göttingen, Göttingen, 1997)
49. K.O. Kongshaug, H. Fjellvåg, Inorg. Chem. **45**, 2424 (2006)

50. Y.L. Hu, M.L. Ding, X.Q. Liu, L.B. Sun, H.L. Jiang, Chem. Commun. **52**, 5734 (2016)
51. V. Colombo, S. Galli, H.J. Choi, G.D. Han, A. Maspero, G. Palmisano, N. Masciocchic, J.R. Long, Chem. Sci. **2**, 1311 (2011)
52. J. Duan, M. Higuchi, S. Horike, M.L. Foo, K.P. Rao, Y. Inubushi, T. Fukushima, S. Kitagawa, Adv. Funct. Mater. **23**, 3525 (2013)
53. J. Duan, M. Higuchi, R. Krishna, T. Kiyonaga, Y. Tsutsumi, Y. Sato, Y. Kubota, M. Takatae, S. Kitagawa, Chem. Sci. **5**, 660 (2014)
54. Y.N. Gong, T. Ouyang, C.T. He, T.B. Lu, Chem. Sci. **7**, 1070 (2016)
55. J. Dong, P. Cui, P.F. Shi, P. Cheng, B. Zhao, J. Am. Chem. Soc. **137**, 15988 (2015)
56. J. Cui, Y. Li, Z. Guo, H. Zheng, Chem. Commun. **49**, 555 (2013)
57. H.R. Fu, F. Wang, J. Zhang, Dalton Trans. **44**, 2893 (2015)
58. M.D. Allendorf, C.A. Bauer, R.K. Bhakta, R.J.T. Houk, Chem. Soc. Rev. **38**, 1330 (2009)
59. J. Heine, K. Muller-Buschbaum, Chem. Soc. Rev. **42**, 9232 (2013)
60. S.J.A. Pope, B.J. Coe, S. Faulkner, E.V. Bichenkova, X. Yu, K.T. Douglas, J. Am. Chem. Soc. **126**, 9490 (2004)
61. F.N. Dai, H.Y. He, D.L. Gao, F. Ye, D.F. Sun, Z.J. Pang, L. Zhang, G.L. Dong, C.Q. Zhang, Inorg. Chim. Acta **362**, 3987 (2009)
62. S.S. Nagarkar, A.V. Desai, S.K. Ghosh, Chem. Commun. **50**, 8915 (2014)
63. X.-Z. Song, S.-Y. Song, S.-N. Zhao, Z.-M. Hao, M. Zhu, X. Meng, L.-L. Wu, H.-J. Zhang, Adv. Funct. Mater. **24**, 4034 (2014)
64. J.-D. Xiao, L.-G. Qiu, F. Ke, Y.-P. Yuan, G.-S. Xu, Y.-M. Wang, X. Jiang, J. Mater. Chem. A **1**, 8745 (2013)
65. S. Barman, J. Anand Garg, O. Blacque, K. Venkatesan, H. Berke, Chem. Commun. **48**, 11127 (2012)
66. J.A.A. Ho, H.C. Chang, W.T. Su, Anal. Chem. **84**, 3246 (2012)
67. J.S. Qin, S.J. Bao, P. Li, W. Xie, D.Y. Du, L. Zhao, Y.Q. Lan, Z.M. Su, Chem. Asian J. **9**, 749 (2014)
68. P. Wu, Y. Liu, J. Wang, Y. Li, W. Liu, Inorg. Chem. **54**, 11046 (2015)
69. F.S. Shan, J.P. Lai, H. Sun, P. Zhang, C. Luo, Y.H. He, H.R. Feng, RSC Adv. **6**, 66215 (2016)
70. F. Xu, L. Kou, J. Jia, X. Hou, Z. Long, S. Wang, Anal. Chim. Acta **804**, 240 (2013)
71. J. Yang, Z. Wang, Y. Li, Q. Zhuang, W. Zhao, J. Gu, RSC Adv. **6**, 69807 (2016)
72. Z.Y. Guo, H. Xu, S.Q. Su, J.F. Cai, S. Dang, S.C. Xiang, G.D. Qian, H.J. Zhang, M. O'Keeffe, B.L. Chen, Chem. Commun. **47**, 5551 (2011)
73. S. Dang, E. Ma, Z.S. Sun, H.J. Zhang, J. Mater. Chem. **22**, 16920 (2012)
74. W. Lu, X. Qin, S. Liu, G. Chang, Y. Zhang, Y. Luo, A.M. Asiri, A.O. Al-Youbi, X. Sun, Anal. Chem. **84**, 5351 (2012)
75. B. Jurado-Sánchez, A. Escarpa, J. Wang, Chem. Commun. **51**, 14088 (2015)
76. N.D. Rudd, H. Wang, E.N.A. Fuentes-Fernandez, S.J. Teat, F. Chen, G. Hall, Y.J. Chabal, J. Li, ACS Appl. Mater. Interfaces **8**, 30294 (2016)
77. H.J. Cheng, H.X. Tang, Y.L. Shen, N.N. Xia, W.Y. Yin, W. Zhu, X.Y. Tang, Y.S. Ma, R.X. Yuan, J. Solid State Chem. **232**, 200 (2015)
78. J.M. Hu, R. Guo, Y.G. Liu, G.H. Cui, Inorg. Chim. Acta **450**, 418 (2016)
79. H.X. Qi, J.F. Wang, Z.G. Ren, J.J. Ning, J.P. Lang, Dalton Trans. **44**, 5662 (2015)
80. F. Wang, F.L. Li, M.M. Xu, H. Yu, J.G. Zhang, H.T. Xia, J.P. Lang, J. Mater. Chem. A **3**, 5908 (2015)
81. Y. Gong, P.G. Jiang, Y.X. Wang, T. Wu, J.H. Lin, Dalton Trans. **42**, 7196 (2013)
82. F. Wang, Z.S. Liu, H. Yang, Y.X. Tan, J. Zhang, Angew. Chem. Int. Ed. **50**, 450 (2011)
83. Z.L. Wu, C.H. Wang, B. Zhao, J. Dong, F. Lu, W.H. Wang, W.C. Wang, G.J. Wu, J.Z. Cui, P. Cheng, Angew. Chem. Int. Ed. **54**, 1 (2016)